Interplay between transport, magnetic, and ordering phenomena in $Sm_{1-x}Ca_xMnO_3$

J. Hejtmánek, Z. Jirák, and M. Maryško
Institute of Physics of ASCR, Cukrovarnická 10, 16200 Praha 6, Czech Republic

C. Martin, A. Maignan, M. Hervieu, and B. Raveau
Laboratoire CRISMAT, UMR 6508 Associe au CNRS, ISMRA et Université de Caen 6, Boulevard du Maréchal Juin, 14050 Caen Cedex, France

(Received 1 July 1999)

We present the detailed study of $Sm_{1-x}Ca_xMnO_3$ with $0.3 \leqslant x \leqslant 1$ probed by electrical resistivity, thermoelectric power, magnetic susceptibility, and thermal conductivity measurements between 10 and 320 K. The transport and thermal data are analyzed supposing polaronic carriers and explanation of experimental results is made in coherence with ordering phenomena recently evidenced by electron diffraction and lattice imaging. Sample $Sm_{0.7}Ca_{0.3}MnO_3$ an is insulating ferromagnet without any obvious transport anomalies at $T_C \cong 95$ K. Contrary to that, the compounds with $0.4 \leqslant x \leqslant 0.75$ exhibit, at critical temperature T_{crit}, distinct anomalies in transport and magnetism. Respecting the recent electron microscopy results, these anomalies can be associated to the real space charge ordering of Mn^{3+}/Mn^{4+} ions, i.e., $T_{crit} = T_{CO}$. Our experimental data indicate, however, that long-range antiferromagnetic order likely develops at $T_N \sim 130$ K, i.e., well below T_{CO}. The $Sm_{0.2}Ca_{0.8}MnO_3$ sample is a *C*-type antiferromagnet with *p*-type conductivity at low temperatures. For the samples with $x \sim 0.9$, the paramagnetic highly conducting state is replaced below $T_{crit} = 110$ K by a ''cluster glass'' ferromagnetic state. The series is completed by a *G*-type $CaMnO_3$ antiferromagnet with $T_N = 122$ K. In all studied samples, the heat is conducted mainly by phonons with the mean free path critically limited in dependence of composition and temperature by scattering on impurities (Sm/Ca substitution), dynamic and/or static Jahn-Teller modes and spin fluctuations. Nevertheless, for the samples with $0.6 \leqslant x \leqslant 0.9$, which exhibit high electrical resistivity in the paramagnetic state, the thermal conductivity at room temperature comprises significant electronic contribution. [S0163-1829(99)01744-0]

I. INTRODUCTION

The detailed electron diffraction and lattice imaging study of $Sm_{1-x}Ca_xMnO_3$ system with $0.4 \leqslant x \leqslant 0.85$, complemented by electrical resistivity and magnetization, has been published very recently.[1] Moreover, we have implemented the magnetic and transport study of calcium rich manganites $Sm_{1-x}Ca_xMnO_3$, with $0.85 \leqslant x \leqslant 1.0$.[2] Even a relatively small injection of carries in the parent $CaMnO_3$ antiferromagnetic insulator ($T_N = 122$ K) has been shown to lead simultaneously to metalliclike charge carrier transport in the paramagnetic state and to appearance of ferromagnetic component below 110 K. The magnetic state in this compositional range was described as a cluster glass and is restricted to a compositional range close to $x \sim 0.9$. Magnetic moment at 10 K increases from 0.05 μ_B/Mn for $x = 0.975$, peaks to 1.15μ_B/Mn for $x = 0.88$ and abruptly decreases for $x \leqslant 0.86$ ($M \leqslant 0.01 \mu_B$/Mn).[2] The charge carrier transport in the paramagnetic state in this compositional range was explained supposing polaronic carries with mobility strongly influenced by random potential fluctuations due to chemical substitution. Nevertheless the polaron binding energies remain small ($\sim 10^0$ meV) thus leading to the metalliclike temperature dependence of the resistivity. Except of $x = 0.88$ sample, exhibiting highest magnetic moment, the chemical disorder together with magnetic frustration lead to thermally activated electrical resistivity below characteristic temperature T_{CG}. Only small resistivity and thermopower anomalies observed at T_{CG} indicated, however, that electrons are not subject to such a fundamental change of behavior as in hole doped colossal magnetoresistance (CMR) counterparts.

For lower calcium concentrations, i.e., $0.4 < x < 0.85$, the situation is essentially different. The charge ordering (CO) phenomena appear and different types of order, in dependence of chemical composition, have been proposed: (i) short-range ($x \sim 0.8$), long-range charge ordering either commensurate or incommensurate with a modulation q vector close to x ($0.5 \leqslant x \leqslant 0.75$) and ''partially'' charge ordered state in which single ''Mn^{3+}'' layers alternate with mixed ''Mn^{3+}/ Mn^{4+}'' layers ($0.4 \leqslant x < 0.5$).[1] The onset of the CO (T_{CO}) was shown to coincide with an increase of electrical resistivity and decrease of magnetic moment. Studies of $Pr_{1-x}Ca_xMnO_3$ and $La_{-1-x}Ca_xMnO_3$ solid solutions have shown, however, that long-range antiferromagnetic (AF) order, which should naturally follow the CO, is established well below the T_{CO}.[3,4] For the $Sm_{0.5}Ca_{0.5}MnO_3$ single crystal $T_N \sim 160$ K were claimed.[5]

In present paper, we study the charge carrier and heat transport in $Sm_{1-x}Ca_xMnO_3$ polycrystalline system with $0.3 < x < 1$ and we make attempt to intercorrelate the anomalies observed in charge carrier and thermal transport and magnetic susceptibility with ordering phenomena. Furthermore, the thermoelectric power and thermal conductivity data are not, unlike to electrical resistivity, fundamentally influenced by a polycrystalline nature of the specimens and enable a better insight into the intrinsic properties of respective material.

II. EXPERIMENT

The synthesis of polycrystalline samples using stoichiometric mixtures of Sm_2O_3, CaO and Mn_2O_3 described previously.[2,6,7] The mixtures with nominal compositions $Sm_{1-x}Ca_xMnO_3$ were first heated at 1000 °C to achieve decarbonation, sintered at 1500 °C for 12 h and slowly cooled down to room temperature. Purity and cationic homogeneity were systematically checked by electron diffraction coupled with energy dispersive spectroscopy (EDS) analysis.

The electric resistance measurements were performed from room temperature down to 4 K with a quantum design physical properties measurement system in the earth magnetic field. The magnetic susceptibility data were collected with a quantum design superconducting quantum interference device (SQUID) ac-dc magnetometer or ACS 7000 Lake Shore susceptometer. Applied magnetic field h_{ac} was within the range of $1Oe \leqslant h_{ac} \leqslant 10Oe$ and excitation frequency between 10 and 100 Hz.

The thermoelectric power and thermal conductivity measurements were carried out between 11-320 K using close-cycle refrigerator. The four point steady-state method with separated measuring and power contacts (sample extremities) was applied to eliminate the thermal resistances between the sink and the heater, respectively. The rectangular-shaped sample was mounted on the heat sink of cryostat and the miniature resistor heater, charged using a pair of 0.003 in. chromel wires, was stuck by general electric (GE) varnish on the end of the sample. The temperature gradient and voltage drop was monitored using two separated differential chromel-constantan thermocouples (0.003 in. in diameter) which were affixed to the sample using copper link, indium solder, and silver paint. A typical temperature difference across the sample was 1.5 K. The influences of the thermopower of chromel, in case of thermovoltage measurement, and sample radiation, and thermal conductivity of differential thermocouples, in case of thermal conductivity measurement, were carefully taken into account and corresponding corrections were made. The experimental setup was checked using reference samples (superconducting Bi-2223 ceramics, chromel, plexiglass, . . .) and the error within all range of temperatures did not exceed absolutely $\sim 1\ \mu V\,K^{-1}$ (thermopower) and $\sim 0.1\ W\ m^{-1}\ K^{-1}$ (thermal conductivity) or relatively of 5% of measured value.

III. RESULTS AND DISCUSSION

The transport properties of the $Sm_{1-x}Ca_xMnO_3$ samples for $0.3 \leqslant x \leqslant 1.0$ below room temperature are exemplified in Figs. 1 and 2, where the temperature dependence of the electrical resistivity and thermoelectric power are shown, respectively. With respect to a close correlation between transport and magnetic properties the magnetic susceptibility data, displayed on Figs. 3 and 4, are discussed concurrently.

All studied samples, except that with $x \sim 0.9$, are insulating at low temperatures. The overview of main transport characteristics in paramagnetic state confronted with chemical composition is given in the Table I; used approaches and formulas are summarized in Annexe. The $Sm_{0.7}Ca_{0.3}MnO_3$ sample is insulating in the all studied temperature region. The activation energy of the resistivity of about 150 meV is temperature independent and thermoelectric power is large and positive - see Table I. The activation energy of thermopower of ~ 35 meV remains, however, substantially lower than that of electrical resistivity. This behavior is consistent with a small polaron mechanism of carrier transport dominated by carrier hopping. When the calcium concentration is increased the transport properties gradually change; metallicklike variation starts to dominate the temperature dependence of resistivity, the absolute value of thermoelectric power decreases and its temperature dependence smoothly changes from temperature activated via temperature independent to that typical for metals. i.e. linearly decreasing with decreasing temperature - see Figs. 1 and 2. This compositional variation indicates that the carrier activation energy W_ρ, gradually and smoothly decreases with increasing calcium doping-see Table I. Taking into account the structural aspects we can correlate this tendency to decreasing average distortion on MnO_6 network, tied to decreasing concentration of Mn^{3+} ions. This results simultaneously to suppression of Jahn-Teller (J.T.) effect and, consequently, in expense of decreasing activation energy, the temperature-

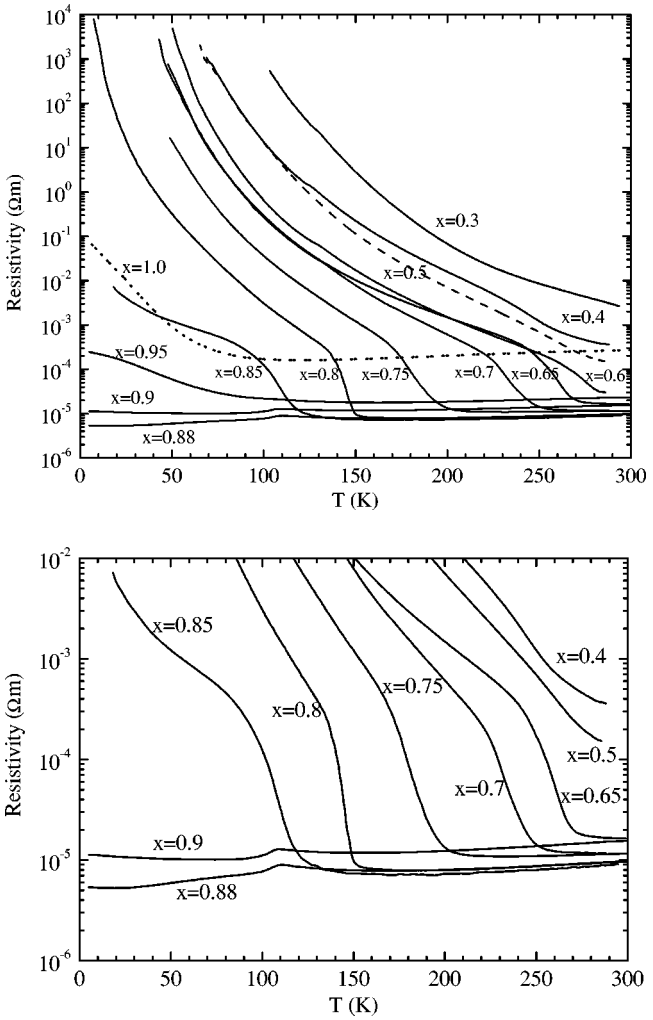

FIG. 1. Temperature dependence of the electrical resistivity for the $Sm_{1-x}Ca_xMnO_3$ series with $0.3 \leqslant x \leqslant 1$ (x values are labeled on the graph). In the sake of clarity the dashed line ($x=0.5$) and dotted line ($x=1.0$) are used in the upper panel. In the lower panel the metal-insulator transition tied to charge-ordering ($0.4 \leqslant x \leqslant 0.85$) or anomalies due to magnetic ordering ($x \sim 0.9$) are emphasised.

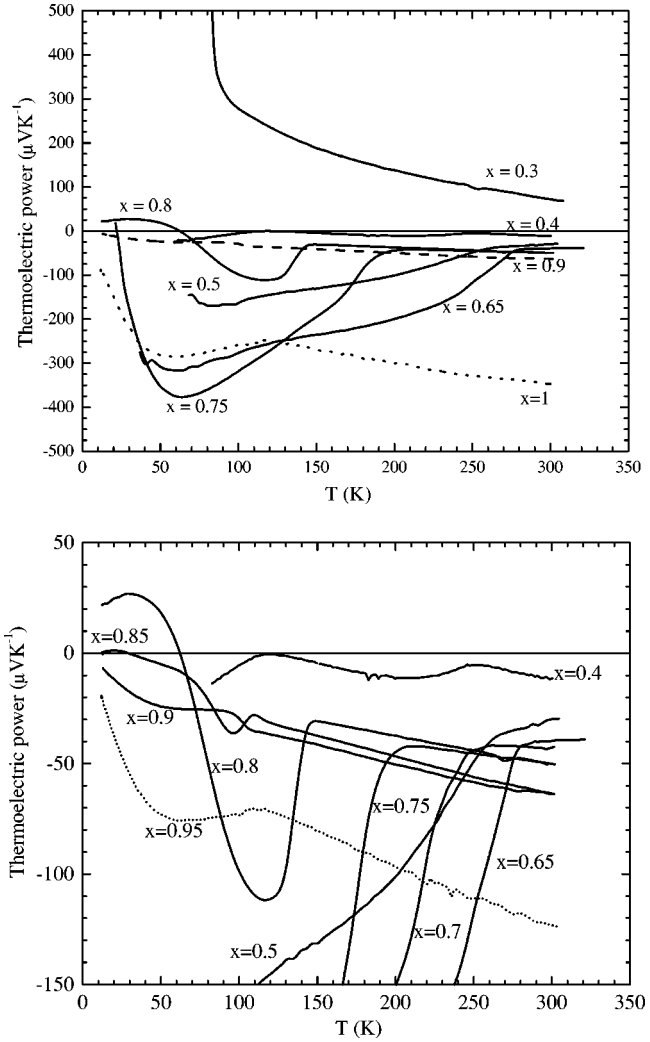

FIG. 2. Temperature dependence of the thermoelectric power for the selected samples of $Sm_{1-x}Ca_xMnO_3$ series -x values are labeled on the graph. In the sake of clarity the dashed line ($x=0.9$) and dotted line ($x=1.0$) are used in the upper panel. In the lower panel the anomalies in the temperature dependence for all studied samples between $0.4 \leqslant x \leqslant .95$ are shown in detail.

dependent carrier scattering starts to limit the transport in calcium rich samples.

When lowering the temperature below 300 K a clear anomaly in the temperature dependencies of resistivity, thermopower and magnetic susceptibility for samples with $0.4 \leqslant x \leqslant 0.85$ is observed - see Figs. 1, 2, and 3. Such type of metal - insulator transition was already observed and linked to orbital and charge-ordering phenomena with characteristic temperature claimed as charge ordering temperature T_{CO}.[1,3] The steep onset of carrier localization below T_{CO} is evidenced in lower panels of Figs. 1 and 2. The temperature dependence of magnetic susceptibility, displayed in Fig. 3, exhibits a peak at T^{max} which sharpness increases with increasing x. A marked decrease of magnetic susceptibility below T^{max} is indicative for the cut off the ferromagnetic interactions due to orbital-(charge-) ordering process. The sharpness of magnetic transition coincide with the resistivity data; broader maximum of $\chi = f(T)$ for $x=0.4$ and 0.5 samples harmonises with diffusive character of resistivity and thermopower transitions while samples with higher x

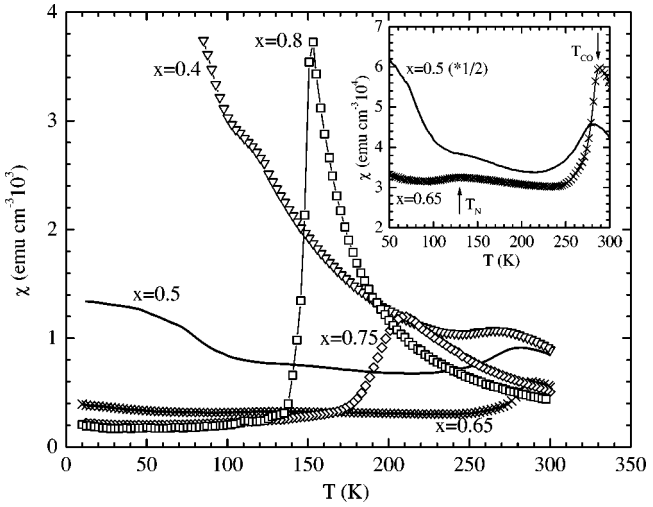

FIG. 3. Temperature dependence of the initial susceptibility for $Sm_{1-x}Ca_xMnO_3$ series - x values are labeled on the graph. In the inset the detail of a sharp drop at T_{CO} and a broad bump at T_N for $Sm_{0.5}Ca_{0.5}MnO_3$ $(--)$ and $Sm_{0.35}Ca_{0.65}MnO_3$ $(\times)$ are shown.

present sharp anomalies in these physical quantities. Below the characteristic temperature a weakly temperature-dependent negative thermopower is accompanied by a temperature activated resistivity.

The electrical resistivity in the paramagnetic state for the $1.0 \leqslant x \leqslant 0.65$ compounds is characterized by a semi-metallic behavior with small activation enrgy of ''hopping'' polarons. This activation energy, however, increases with increasing Sm concentration from 5.4 meV, estimated for $x=1.0$ up to 158 meV for $x=0.3$ - see Table I. This phenomenon reflects the increasing tendency to polaron formation with increasing x as mentioned before in more detail in Ref. 2. To illustrate comparative insight in carrier transport for all studied samples up to $x=0.85$, the temperature dependence of the local activation energy W_{local} of the resistivity, defined as $W_{local} = d(ln\rho)/d(^1/_T)*k_B$, was plotted in Fig. 5. The composition dependence of the peak temperature T^{max}, illus-

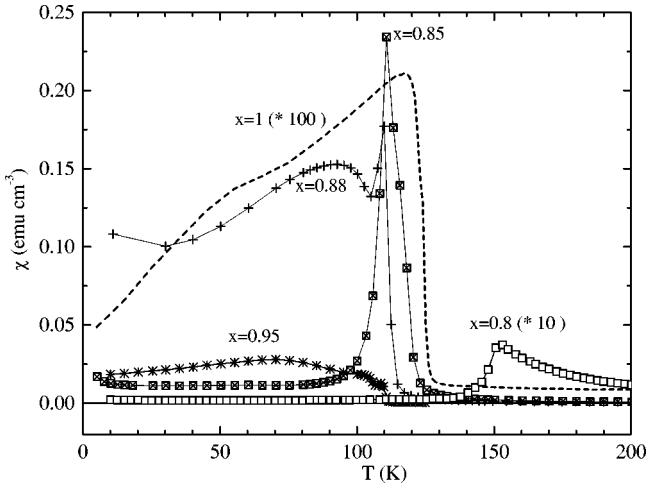

FIG. 4. Temperature dependence of the initial susceptibility for samples with significant spontaneous ferromagnetic component $(0.85 \leqslant x \leqslant 0.95)$. For the comparison magnified curves for nearly pure Mn^{4+} $CaMnO_3$ $(\cdots)$ and $Sm_{0.2}Ca_{0.8}MnO_3$ (-□-) are also shown.

TABLE I. Critical temperatures and some transport characteristics (in paramagnetic state) of the $Sm_{1-x}Ca_xMnO_3$ series deducted or calculated from transport and magnetic measurements. The critical temperature T_{crit} or charge ordering temperature T_{CO} were averaged from transport and magnetic measurements. The magnetic (T_{CG}, T_C or T_N) ordering temperatures were estimated on a base of anomalies found in thermopower and magnetic susceptibility and the $n(Mn)/n(Mn^{3+})$ ratio was calculated according the chemical composition. A more detailed description of evaluated W_ρ^{300K}, $N(E)/n$, and E_s is given in the Appendix.

x	T_{crit} or T_{CO}(K) (T_{MAG})(K)	$\rho_{(300K)}$ (mΩ cm)	W_ρ^{300K} (meV)	α^{300K} (μV K^{-1})	$N(E)/n$ E_s (meV)	$\frac{n(Mn)}{n(Mn^{3+})}$
0.30	(T_C=95)	268	158	+70	1.4$^\sharp$ 45 meV	1.4
0.40	T_{CO}~225 (T_N~125)	37	150	−12	1.6$^\sharp$ 10 meV	1.7
0.50	T_{CO}~275 (T_N~140)	15	~85$^+$	−30	2.1* 2.3$^\sharp$	2
0.60	T_{CO}~287 (T_N~135)	3		−36	2.2* 2.5$^\sharp$	2.5
0.65	T_{CO}~275 (T_N~130)	1.7	~35	−39	2.3* 2.57$^\sharp$	2.85
0.70	T_{CO}~240 (T_N~130)	1.2	31	−43	3	3.3
0.75	T_{CO}~196 (T_N~135)	1.2	15	−50	5.5	4
0.80	T_{crit}~150	0.97	12	−52	7	5
0.85	T_{crit}~115	0.92	11	−62	9	6.5
0.88	(T_{CG}=110)	1.0	10.3	−65	7	7
0.90	(T_{CG}=110)	1.5	8.4	−65	10	10
0.95	(T_{CG}=110)	2.33	8.1	−120	12	20
1.0	(T_N=122)	26.9	5.4	−350	22	

*β

$^\sharp\beta$=1 (see Appendix)

$^+$Estimated from high-temperature data.

trated in lower panel of Fig. 5, increases from 110 K for x = 0.85 up to 285 K for x = 0.60 and then decreases to 240 K for x = 0.40. The similar composition evolution found for the local activation energy W_{local} determined at 50 K, well below T^{max}, corroborates a strong coupling between charge carriers and lattice.

The absolute values of the local activation energy cannot be analyzed quantitatively. Supposing the similar microstructure of studied specimens we can compare, however, the shape of the peaks in Fig. 5. The small absolute values and large width of peaks for x = 0.4 (at 245 K) and x = 0.5 (at 265 K) samples corresponds likely to diffusive character of the transition previously demonstrated for $Pr_{0.5}Ca_{0.5}MnO_3$.[8] The increasing height of the peak for x > 0.5 samples is coherent with increasing sharpness of phase transition. A small peak and small activation energy of electrical resistivity at low temperatures of x = 0.85 sample is consistent with its CMR behavior. A small decrease of the activation energy around 125 K, shown in the upper panel of Fig. 5, appears for samples with x = 0.4 and 0.5. This is likely a consequence of residual ferromagnetic order, which was reported in this compositional range.[3] This hypothesis is supported by temperature dependence of magnetic susceptibility, which increases with lowering temperature - see Fig. 3. Moreover for samples with $0.6 < x < 0.8$, where any indication of ferromagnetism at low temperatures were not reported up to now, neither resistive anomaly nor increasing magnetic susceptibility are observed - see Fig. 3 and inset of Fig. 5.

In the compositional range where charge order sets in, i.e., for $0.4 < x < 0.75$, we have registered additional bump in the susceptibility behavior at temperatures significantly below T_{CO}—see inset of Fig. 3. In pioneer study of $Pr_{1-x}Ca_xMnO_3$ solid solution one of us has claimed that that long-range antiferromagnetic order can be stabilized significantly below T_{CO} (T_{CO}~250 K and T_N~180 K for $0.4 < x < 0.75$).[3] This observation of separation of T_{CO} and T_N was more recently confirmed by detailed neutronographic and magnetic studies of $La_{1/3}Ca_{2/3}MnO_3$ (T_{CO}=270 K and T_N~170 K) and $Pr_{0.5}Ca_{0.5}MnO_3$ (T_{CO}=245 K and T_N~175 K).[9,10] For the last compound a similar bump in the

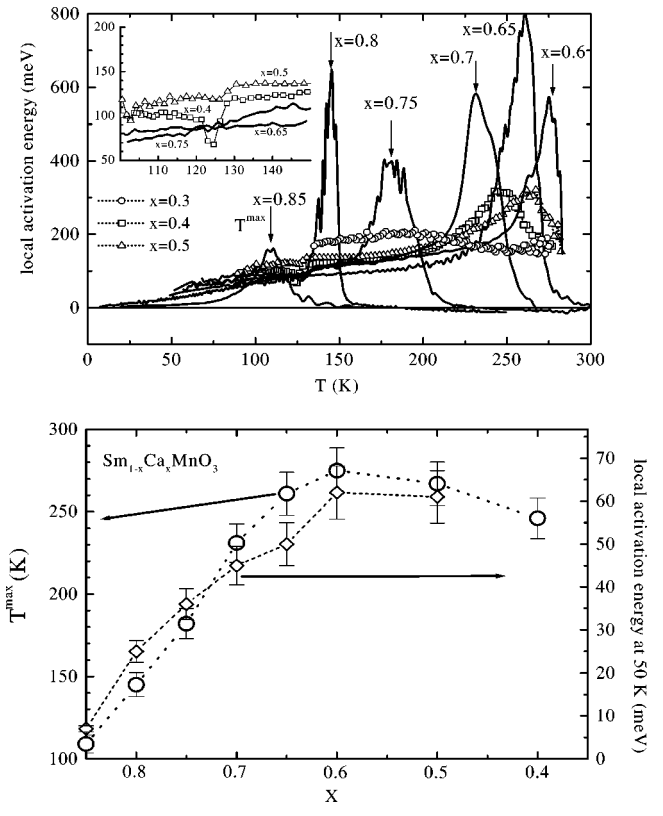

FIG. 5. - Temperature dependence of the local activation energy W_{local} observed as a slope of $ln(\rho)=f(T^{-1})$ dependence ($W_{local}={}^{d(ln(\rho))}/_{d(T^{-1})}$) for $Sm_{1-x}Ca_xMnO_3$ series (x values are labeled on the graph). In the inset the temperature dependence of W_{local} between 100 and 150 K for selected samples is shown in detail. In the lower panel the concurrence between the composition dependence of T_{max} (left) and local activation energy W_{local} at 50 K (right) for $Sm_{1-x}Ca_xMnO_3$ series.

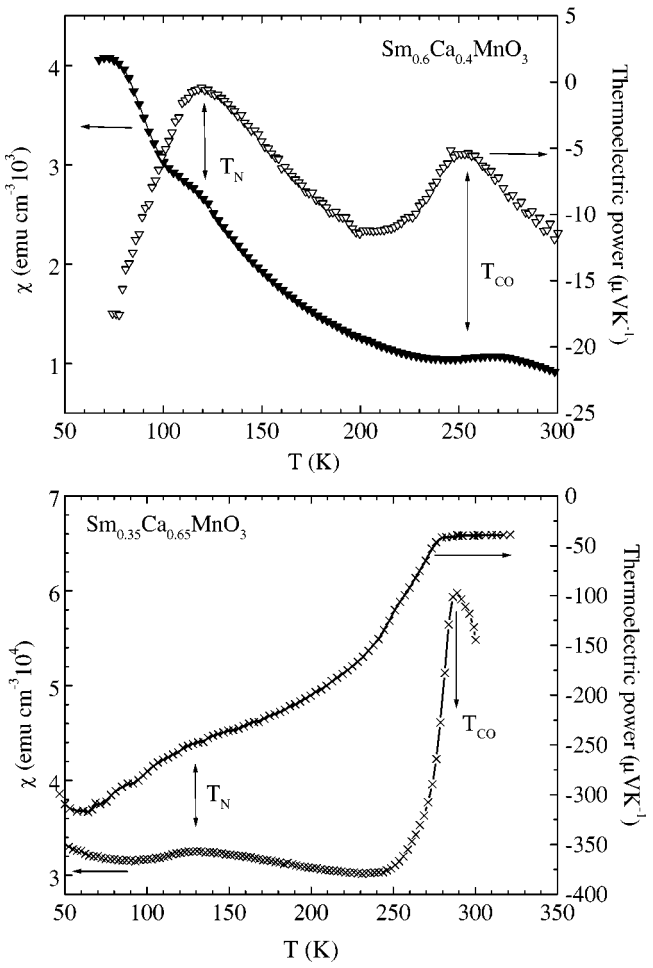

FIG. 6. The temperature dependence of the magnetic susceptibility and thermoelectric power for $Sm_{0.6}Ca_{0.4}MnO_3$ and $Sm_{0.35}Ca_{0.65}MnO_3$. The distinct anomalies in the temperature evolution enable to distinguish between T_{CO} and T_N.

magnetic susceptibility in the vicinity of neutronographically determined T_N was observed. Consequently, we associate the broad bump in the susceptibility, depicted in detail in the inset of Fig. 3, with a long-range AF order with $T_N \sim 135$ K. The long-range AF order should naturally influence the carrier transport and we can explore, as an independent probe, the thermoelectric power temperature dependencies. Indeed, the thermoelectric power curves for $0.4 \leqslant x \leqslant 0.75$ samples exhibit in a very vicinity of presumed T_N a clear anomaly. This situation is exemplified for two compositions in Fig. 6. The decrease of thermopower below ~ 130 K signifies the onset of additional energy barrier further inhibiting the carrier transport. The outstanding coincidence of the anomalies observed simultaneously in both the magnetic susceptibility and thermopower seems to confirm the trustworthiness of the hypothesis that long-range AF order setsup independently on chemical composition at $T_N \sim 135$ K, i.e., significantly below T_{CO}. Below the T_N, the thermoelectric power further decreases and reaches minimal values at ~ 60 K. Supposing that both spin and orbital degeneracy are quenched at this temperature (see Annexe) we can use a simple Heikes approximation to estimate the concentration of hopping carriers. The value of $\sim -400\ \mu V\ K^{-1}$ observed for the $Sm_{0.25}Ca_{0.75}MnO_3$ indicates that only of $\sim 4\%$ of Mn^{3+} e_g electrons are free to participate to hopping conduction at this temperature. Finally, we note that the neutronographic measurements, which should unambiguously determine the T_N, are in progress and will be soon published.

The low-temperature transport properties for the next in the series $Sm_{0.2}Ca_{0.8}MnO_3$ sample, however, somewhat differs from that of $0.4 \leqslant x \leqslant 0.75$ series. The sample resistance remains relatively low down to lowest temperatures ($R < 10^7\ \Omega$ at 10 K) and this fact enables to determine the low-temperature thermopower with sufficient accuracy thus revealing very peculiar temperature dependence. Below 150 K, where contrary to samples with $0.4 < x < 0.75$ only a monoclinic distortion and a short-range charge order was detected[1], the thermopower sharply decreases but suddenly below 120 K starts to increase with decreasing temperature, changes sign around 60 K and remains unambiguously positive down to 10 K. Our attempt to explain this behavior is based on recent low-temperature structural data that reveal the existence of the *C*-type antiferromagnetic order, already observed in $Pr_{1-x}Ca_xMnO_3$ system for $x \sim 0.8$, and a regular distortion of MnO_6 network with $3\mathbf{d}_{z^2}$ orbital polarization.[11] Experimentally observed average prolongation of MnO_6 octahedra together with a short-range charge order signify, however, the existence of some MnO_6 octahedra with higher local electron density in $3\mathbf{d}_{z^2}$ orbital than that which can be

deduced from chemical substitution. In other words, there is a disproportion between symmetry requirements, leading to relatively high-electron occupation of $3\mathbf{d}_{z^2}$ orbital and local Mn^{3+}/Mn^{4} order and, on the other side, the average Mn valency determined by chemical substitution. In a frame of this picture the charge transport is realized in ''negatively'' charged MnO_6 network (with respect to average valency of $Mn \sim 3.8+$) by charge compensating positive carriers - holes - which move by hopping. The positive low-temperature thermopower is thus attempted to be explained as a configurational entropy of ''holes'' hopping between ''matrix'' composed of Mn ions which exhibit average Mn valency lower then chemically determined value, i.e., $Mn^{3.8+}$.

The common feature observed for $0.5 \leqslant x \leqslant 0.85$ samples, which was already mentioned, is that the activation energy decreases with decreasing temperature and apparently tends to zero at 0 K. The best model which suits this behavior is variable-range carrier hopping (VRH) in three-dimensions $\varrho \sim \varrho_0 \exp(T_0/T)^{1/4}$, the simple approximation by Arhenius law does not provide the most reliable model of charge carrier transport. In a frame of the VRH model, less energetically demanding conducting channels (tied to, e.g., disorder, defects and imperfections, . . .) open at lower temperatures so carriers ''hop'' to longer distance but between less energetically separated states. Experimentally observed VRH fit of resistivity data for samples with $0.85 \leqslant x \leqslant 0.4$ below appropriate $T_{CO}(T_N)$ provided $10\times$ lower standard deviation than a simple Arrhenius model. The VRH behavior is further supported by thermopower since this, despite of temperature activated resistivity, tends to zero at 0 K thus implying the finite density of states at E_F. A small peak on the resistivity and a drop of thermopower observed for sample with $x = 0.9$ at $T_{CG} \sim 110$ K are correlated with a maximum in magnetic susceptibility (Fig. 4) and likely linked to cluster glass ferromagnetism appearing below $T_{CG} = 110$ K. Finally let us mention that the CMR properties of $x = 0.85$ sample originate from its frontier position between insulating *C*-type antiferromagnetism and metallic cluster glass ferromagnetism.

When the calcium concentration is further increased up to $x = 0.95$, lower magnetic susceptibility, higher electrical resistivity and increased absolute value of thermopower concurrently indicate the decrease of ferromagnetic interactions at the expense of antiferromagnetic ones. The decrease of the thermopower and the peak on the susceptibility for $CaMnO_3$ signifies a long-range AF order at $T_N = 122$ K. Similar values of thermoelectric power observed for $CaMnO_3$ and $Sm_{0.25}Ca_{0.75}MnO_3$ at ~ 60 K imply, supposing the same mechanism of charge-carrier transport, the comparable charge-carrier concentration in both compounds. The absence of disorder induced by cationic substitution and no charge and/or orbital order leads, however, to much higher carrier mobility in $CaMnO_3$; the electrical conductivity is more then 10^3 times higher then that of compared $Sm_{0.25}Ca_{0.75}MnO_3$ - see Fig. 1.

With respect to a close interrelation between the transport and lattice effects the thermal transport probed by thermal conductivity measurements was also studied. In order to compare and analyze the data measured on samples of different compactness the data displayed in Fig. 7 were corrected on the sample porosity.[12] Logarithmic scale used in the upper panel enables to depict the thermal conductivity for all series since Sm substitution induces the dramatic decrease of its absolute value. The blowup in the lower panel exemplifies the anomalies accompanying charge or spin ordering, respectively.

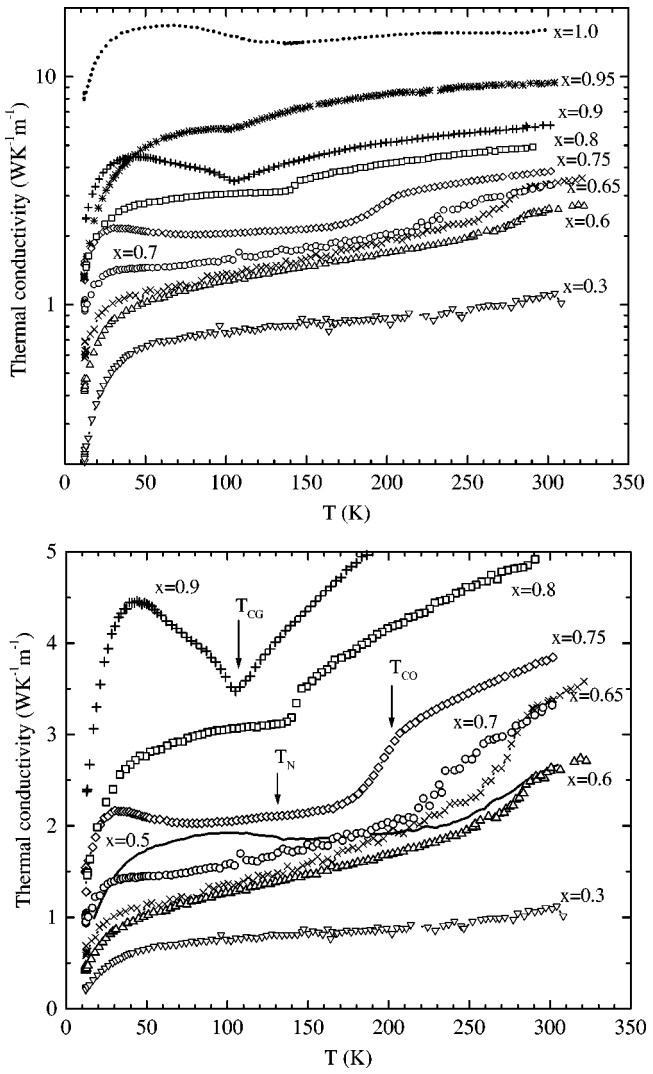

FIG. 7. Temperature dependence of the thermal conductivity for the $Sm_{1-x}Ca_xMnO_3$ series with $0.3 \leqslant x \leqslant 1$. The values were corrected on the sample porosity and the radiation. The magnification shown in the lower panel enables to visualise the anomalies observed at characteristic temperatures. Samarium concentration x is labeled on the graph.

In conformity with previous studies the thermal conductivity λ in supposed to be confined essentially to its phonon part λ_{phonon} with phonon mean-free path l_{phonon} critically limited by static and/or dynamic Jahn-Teller modes.[13–15] Apart from this phenomenon additional scattering sources of phonons should be considered - namely scattering by impurities (with respect to chemical substitution) and scattering on disordered spins. The interplay of above mentioned phenomena keeps the phonon mean free path very short in all studied temperature range and conventional 1/T dependence with low-temperature peak, characteristic for heat carried by phonons with a mean free path limited by ordinary anharmonic decay, is not observed. Due to concurrently observed

high electrical and small thermal conductivities for $0.6 \leqslant x \leqslant 0.9$ we cannot exclude, however, that overall thermal conductivity λ_{total} comprises a substantial part of electronic contribution $\lambda_{electron}$. The upper limit of the potential magnon contribution λ_{magnon} to λ_{total}, based on magnetic specific heat anomaly of ferromagnetic insulator $La_{0.9}Ca_{0.1}MnO_3$, was estimated by Cohn et al. to $\lambda_{magnon} \leqslant 4*10^{-2}$ W K^{-1} m^{-1} at $\sim$100 K and $\lambda_{magnon} \leqslant 0.1$ W K^{-1} m^{-1} at $\sim$260 K and is neglected in our analysis.[14] As we have mentioned the interplay of strong scattering of phonons on impurities, dynamic J.T. modes and/or static J.T. deformations is likely responsible for both small values of λ_{total} and its decrease with increasing Sm concentration - see Fig. 7. For the least conducting $Sm_{0.7}Ca_{0.3}MnO_3$ sample the observed value of $\lambda_{total} \sim 1$ W m^{-1} K^{-1} is comparable with glassy materials and imply the phonon mean-free path equivalent to Mn-Mn distance. The thermal conductivity of $Sm_{0.5}Ca_{0.5}MnO_3$ sample smoothly decreases below room temperature and exhibits only a broad maximum around 100 K without any other pronounced anomaly below room temperature. In conformity with electric transport and magnetic susceptibility measurements this behavior likely reflects the diffusive character of evolution of charge-ordered state below the onset temperature $T_{CO} \sim 275$ K, which is fully developed only below Nel temperature presumed at $T_N \sim 140$ K. Similar thermal conductivity evolution was previously observed for $Pr_{0.5}Ca_{0.5}MnO_3$ and correlated with structural evolution and long-range AF order.[8,16]

The thermal conductivity of $0.6 \leqslant x < 0.75$ samples behaves differently since a pronounced anomaly at temperatures, clearly associated with the onset of charge-ordering temperature T_{CO}, is registered- see Fig. 7. With respect to a high electrical conductivity above T_{CO}($\sigma_{300K} \sim 10^5 \Omega^{-1}$ m^{-1}) we should consider the electronic contribution $\lambda_{electron}$ as an eventual origin leading to the decrease of λ_{total} in the electrically insulating state. Let us mention that contrary to this assumption the steep increase of thermal conductivity registered below T_C in the metallic state for some ferromagnetic manganites with $\sim$30% Mn^{3+} was definitely not explained by electronic contribution.[8,13,14] To clarify this apparent discrepancy we have attempted to estimate the electronic part $\lambda_{electron}$ for selected samples of $Sm_{1-x}Ca_xMnO_3$ series and a single-crystal $Pr_{0.65}Ca_{0.21}Sr_{0.14}MnO_3$ metallic ferromagnet with two order resistivity decrease at $T_C = 200$ K ($\rho_{205K}/\rho_{200K} = 100$). We have calculated $\lambda_{electron}$ using the Wiedemann-Franz law $\lambda_{electron} = L_o T/\rho$, where $L_o = 2.4*10^{-8}$ W/Ω K^2 is the ideal Lorenz free number and ρ is electrical resistivity. This last quantity was corrected on sample porosity thus providing more reasonable estimate of intrinsic grain resistivity needed for such analysis.[17] The results are shown in the Fig. 8. Experimentally observed Lorenz number for similar ferromagnetic metallic $Ca_{1-x}Sr_xRuO_3$ perovskites is somewhat lower ($L = 1.63*10^{-8}$ W/Ω K^2) and indicates that our estimated electronic contributions should represent rather upper limit of the real $\lambda_{electron}$.[18] Estimated phonon part of thermal conductivity $\lambda_{phonon} = \lambda_{total} - \lambda_{electron}$ reflects the lattice dynamics and clearly differentiate between the smooth evolution of λ_{phonon} over the T_{CO} for $Sm_{0.4}Ca_{0.6}MnO_3$ and

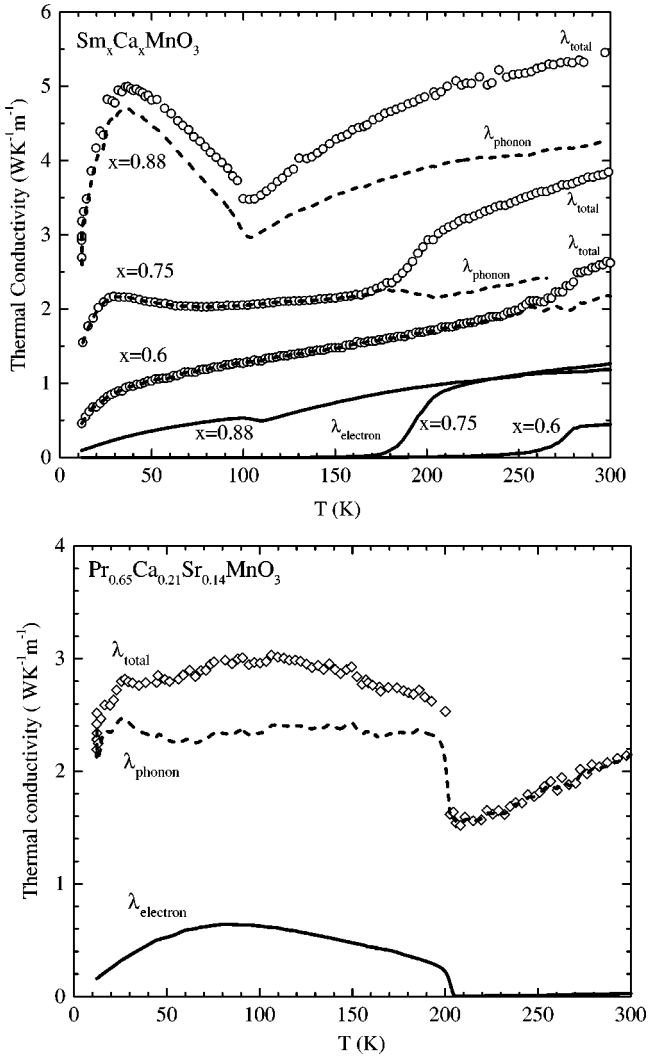

FIG. 8. Temperature dependence of the total thermal conductivity $\lambda_{total} = \lambda_{electron} + \lambda_{phonon}$ for three selected compositions of $Sm_{1-x}Ca_xMnO_3$ series (upper panel) and the ferromagnetic ($T_C = 205$ K) $Pr_{0.65}Ca_{0.21}Sr_{0.14}MnO_3$ single crystal (lower panel). For the separation of phonon and electron parts of thermal conductivity the electronic contribution was estimated using the experimental resistivity data corrected on the sample porosity and supposing the validity of Wiedemann-Franz law.

$Sm_{0.25}Ca_{0.75}MnO_3$ samples and a steep increase at T_C for the $Pr_{0.65}Ca_{0.14}Sr_{0.21}MnO_3$ ferromagnet. Based on this comparison we ascribe the decrease of λ_{total} at T_{CO} in $Sm_{1-x}Ca_xMnO_3$ series to electronic contribution $\lambda_{electron}$ keeping λ_{phonon} almost unaffected by the transition. On the other hand, in agreement with previous studies, the increase observed below M-I transition in ferromagnetic manganites, represented by $Pr_{0.65}Ca_{0.14}Sr_{0.21}MnO_3$ single crystal, should be associated mainly with phonon thermal conductivity. These conclusions seem to be coherent with specific heat measurements observed for $La_{1-x}Ca_xMnO_3$ solid solutions.[19] The peaks $\Delta(c_p)$ observed at $T_{CO} = 270$ K for antiferromagnetic $La_{0.33}Ca_{0.67}MnO_3$ and $T_C = 263$ K for ferromagnetic $La_{0.67}Ca_{0.33}MnO_3$ signifies, that a change of lattice energy is at M-I transition significantly lower at T_{CO} then at T_C.

For ''metallic'' samples $x \sim 0.9$ with ferromagnetic com-

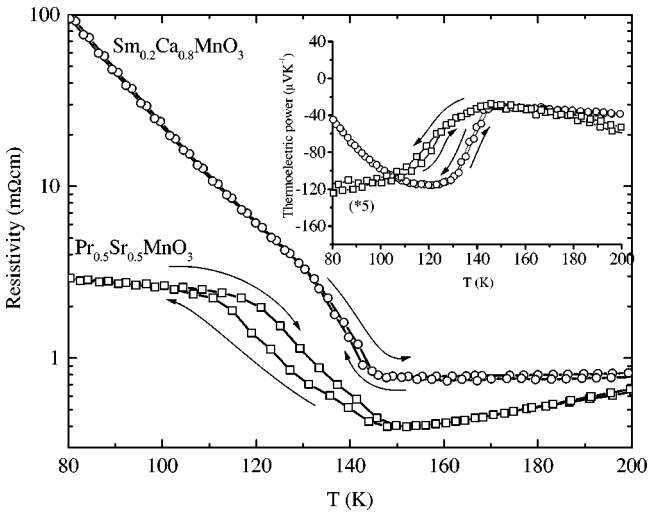

FIG. 9. The comparison of the thermal hysteresis in the resistivity and thermoelectric power (inset) temperature dependencies for polycrystalline $Sm_{0.2}Ca_{0.8}MnO_3$ (○) and single-crystal $Pr_{0.5}Sr_{0.5}MnO_3$ (□), for the sake of comparison the thermopower of $Pr_{0.5}Sr_{0.5}MnO_3$ was five times multiplied. The first order character of the transition in $Pr_{0.5}Sr_{0.5}MnO_3$ at $T_N \sim 150$ K is evidenced by hysteresis both in the resistivity and thermopower.

ponent below $T_{CG}=110$ K the magnetic transition is accompanied by a significant increase of λ at T_{CG}. This tendency is also seen in Sm free *G*-type antiferromagnet $CaMnO_3$. Since the phonon scattering caused both by Ca substitution and J.T. effect of Mn^{3+} ions are much less operational in this compositional range and supposing that phonons are dominating heat carriers (the role of electronic component at low temperatures is negligible), we assert the revival of thermal conductivity below the magnetic ordering temperature to increased phonon mean-free path due to decreased spin scattering below T_N (T_C). Nevertheless the spin wave contribution λ_{magnon} to the thermal conductivity enhancement below T_N (T_{CG}) cannot be unambiguously excluded. To elucidate this question the measurements of magnetothermal conductivity and/or specific heat data are desirable.

The thermal conductivity temperature dependence of $Sm_{0.2}Ca_{0.8}MnO_3$ sample results from its frontier position between two above-mentioned distinct families- metallic cluster glass ferromagnets ($x \sim 0.9$) and charge-ordered antiferromagnets ($0.4 < x \leqslant 0.75$). The thermal conductivity below $T_{crtit} \sim 150$ K is essentially influenced by orbital ordering, which leads to thermal conductivity a decrease due to missing electronic component $\lambda_{electron}$ and, on the other side, to a revival of λ_{phonon} due to increasing phonon mean-free path resulting from orbital and magnetic order. Consequently, the plateau of thermal conductivity observed below 150 K can be understood as an outcome of counteracting roles of the above-mentioned effects.

Despite the sharp resistive transition and abrupt decrease of magnetic susceptibility at $T_{crit} \sim 150$ K, the orbital and magnetic orders in $Sm_{0.2}Ca_{0.8}MnO_3$ are still presumably separated in temperature. This separation should keep the relevant M-I transition rather of the second order. To clarify this, we compare in Fig. 9 the thermal cycling of electrical resistivity and thermoelectric power of $Sm_{0.2}Ca_{0.8}MnO_3$ with $Pr_{0.5}Sr_{0.5}MnO_3$, when for the last one the metal-insulator transition is accompanied by transition from ferromagnetic to antiferromagnetic long-range order at $T_N \sim 150$ K.[20] Clearly observed thermal hysteresis of resistivity and thermoelectric power for the $Pr_{0.5}Sr_{0.5}MnO_3$ sample confirms the first-order character of M-I transition. Contrary to that, the thermal hysteresis is, at least within the experimental error, negligible in the case of $Sm_{0.2}Ca_{0.8}MnO_3$ sample thus supporting the second-order character of the M-I transition.

IV. SUMMARY

The $Sm_{0.7}Ca_{0.3}MnO_3$ sample is the insulating ferromagnet with both thermally activated electrical resistivity and thermoelectric power. For samples with higher calcium concentrations ($0.4 < x \leqslant 0.85$) the polaron binding energy progressively decreases with increasing x and, consequently, the samples with $x > 0.6$ exhibit at room-temperature nonactivated electrical resistivity. When lowering the temperature at certain critical temperature T_{crit} clear anomalies in the temperature dependencies of resistivity, thermoelectric power, magnetic susceptibility, and thermal conductivity are observed. Respecting recent low-temperature electron microscopy results these anomalies can be associated in the $0.4 < x \leqslant 0.75$ compositional range to the real-space long-range charge ordering temperature T_{CO} of Mn^{3+}/Mn^{4+} ions, i.e., $T_{crit}=T_{CO}$, while for the $x=0.8$ sample, the low-temperature data are explained supposing *C*-type orbital polarization and a short-range charge order. A sharp decrease of magnetic susceptibility below T_{CO} together with the carrier localization, demonstrated by electrical resistivity and thermoelectric power, are indicative for the cut off the ferromagnetic interactions, which are mediated by quasi-itinerant carriers. We deduce that antiferromagnetic order, which sets just below T_{CO} is of the short-range and long-range antiferromagnetism develops at T_N well below T_{CO}. The estimated temperature difference ΔT between T_{CO} and T_N seems to be one the largest known in manganites and culminates at $\Delta T \cong 150$ K for $Sm_{0.4}Ca_{0.6}MnO_3$ ($T_{CO}=287$ K and $T_N=135$ K). For $x \sim 0.9$, the paramagnetic ''metallic'' state is at $T_{CG}=110$ K replaced by a cluster glass ferromagnet with a VRH conduction at low temperatures; for the most metallic sample $x=0.88$ the non-activated conductivity is preserved below T_{CO}. The $CaMnO_3$ is an antiferromagnet with $T_N=122$ K.

Unlike to the metal-insulator transition observed in ferromagnetic ''hole-doped'' counterparts (e.g., $Pr_{0.65}Ca_{0.21}Sr_{0.14}MnO_3$) the thermal conductivity temperature dependence for $0.4 < x \leqslant 0.75$ samples does not exhibit such marked discontinuity at metal-insulator transition. For samples with $x > 0.85$, as a result of decreased impact of substitutional disorder and static/dynamic Mn^{3+} Jahn-Teller modes on phonon scattering, spin fluctuations are likely the most important scatters for phonons. The analysis of the experimental data shows that the decrease of thermal conductivity below T_{CO} is likely due to absent electronic component $\lambda_{electron}$ and phonon part λ_{phonon} remains unaffected. Contrary to that, λ_{phonon} seems responsible for the thermal conductivity increase below T_C as in ferromagnetic metallic samples as in ferromagnetic cluster glass samples with $x \sim 0.9$.

ACKNOWLEDGMENTS

We are grateful to Dr. S. Krupička for stimulating discussions. The authors acknowledge the financial support of the Grant Agency of Czech Republic (Grant No. 202-99/0413) and of CNRS, France (PICS Grant No. 280).

APPENDIX

The electrical resistivity in the paramagnetic region was analyzed supposing adiabatic hopping of polaronic carriers $\rho = a^* k_B^* [1-(n/N)]/(n/N)/\omega_o/e^{2*}T^* \exp(W_\rho/k_BT)$ where a is lattice parameter, ω_o is attempt frequency close to optical phonon frequency, n is number of charge carriers, N is the number of available sites and other symbols have their usual meaning. The activation energy of electrical resistivity $W_\rho = E_S + W_H - J$ represent the sum of energy gap E_S, hopping energy W_H, and transfer integral J. Fit of high-temperature ($300\ \mathrm{K} < T < 600\ \mathrm{K}$) data for $Sm_{0.5}Ca_{0.5}MnO_3$ provides an attempt frequency $\omega_O \sim 5^* 10^{13}$ Hz and transfer integral $J \sim 2.5$ meV. These values are in a good agreement with presumed model, at least for this composition. The decrease of W_ρ with increasing x reflects decreasing polaronic effect as due to more favourable tolerance factor of perovskite structure as due to lower concentration of J.T. Mn^{3+} ions.

The temperature dependence of thermoelectric power for samarium-rich samples was described using formula $\alpha = -k_B/|e|^*\{E_s/k_BT + B\}$ where E_S is the energy gap and B represent the configurational entropy term $B = \ln\{[1-(n/N)]/(n/N)\}$. The fact that electron moves in the spin background of distorted MnO_6 octahedra introduces in principle both the spin β_S and orbital β_o degrees of freedom.[21,22] Thus the configurational entropy in a special case of mixed Mn^{3+}/Mn^{4+} valency system can be expressed by simplified form $B = ln\{\beta_S\beta_O[1-(n/N)]/(n/N)\}$ when the spin degree of freedom results in $\beta_S = 5/4$ and β_O results from the interplay of Coulomb interaction, J.T. distortion and thermal energy k_BT. With respect to crystallographic distortion of MnO_6 network observed at room temperature in our analysis only the spin degree of freedom ($\beta_S = 5/4$, labeled *), eventually removed by a short-range magnetic interactions ($\beta_S = 1$, labeled ♯), is considered.[22] The energy gap in the paramagnetic state is observed for $x = 0.3$ and 0.4 samples, the configurational entropy B dominates the region $0.5 \leqslant x \leqslant 0.65$.

In the case of $0.7 \leqslant x \leqslant 1$ samples, the metalliclike resistivity and linear temperature dependence of thermopower allow to use the modified expression for thermopower of single-band metal

$$-\alpha = \pi^{2*} k_B^2/(3e)^* T^* \{N(E)/n + \mathrm{cst.}\}|_{E=E_F}$$

where $N(E)$ is the density of states and n is the carrier density. A plausible width of conduction band of ~ 1 eV (Ref. 23) results in a good agreement between the ratio $N(E)/n$ determined from thermopower and $n(Mn)/n(Mn^{3+})$ calculated from chemical composition thus confirming the reliability of used model—see last two columns of Table I.

[1] M. Hervieu, A. Barnab, C. Martin, A. Maignan, F. Damay, and B. Raveau, Eur. Phys. J. B **8**, 31 (1999).

[2] A. Maignan, C. Martin, F. Damay, B. Raveau, and J. Hejtmánek, Phys. Rev. B **58**, 2758 (1998).

[3] Z. Jirák, S. Krupika, Z. Imsa, D. Dlouh, and Z. Vratislav, J. Magn. Magn. Mater. **53**, 153 (1985).

[4] A. P. Ramirez, S.-W. Cheong, and P. Schiffer, J. Appl. Phys. **81**, 5337 (1997).

[5] Y. Tomioka, A. Asamitsu, H. Kuwahara, Y. Morimoto, M. Kasai, R. Kumai, and Y. Tokura, Physica B **237-238**, 6 (1997).

[6] C. Martin, A. Maignan, F. Damay, M. Hervieu, and B. Raveau, J. Solid State Chem. **134**, 198 (1997).

[7] A. Maignan, C. Martin, F. Damay, and B. Raveau, Chem. Mater. **10**, 950 (1998).

[8] J. Hejtmánek, Z. Jirák, Z. Arnold, M. Maryško, S. Krupika, C. Martin, and F. Damay, J. Appl. Phys. **83**, 7204 (1998).

[9] M. T. Fernndez-Daz, J. L. Martnez, J. M. Alonso, and E. Herrero, Phys. Rev. B **59**, 1277 (1999).

[10] A. Maignan, C. Martin, F. Damay, and B. Raveau, Z. Phys. B: Condens. Matter **104**, 21 (1997).

[11] Z. Jirák and Ch. Martin (unpublished).

[12] M. D. N. Nuez Regueiro and D. Castello, Int. J. Mod. Phys. B **5**, 2003 (1991).

[13] D. W. Visser, A. P. Ramirez, and M. A. Subramanian, Phys. Rev. Lett. **78**, 3947 (1997).

[14] J. L. Cohn, J. J. Neumeier, C. P. Popoviciu, K. J. McClellan, and Th. Leventouri, Phys. Rev. B **56**, R8495 (1997).

[15] J. Hejtmnek, Z. Jirk, S. Krupika, C. Martin, Ch. Simon, A. Maignan, B. Raveau, E. Grivei, and J. P. Issi, J. Appl. Phys. **81**, 4975 (1997).

[16] F. Damay, C. Martin, A. Maignan, M. Hervieu, B. Raveau, Z. Jirak, G. Andre, and F. Bouree, Chem. Mater. **11**, 536 (1999).

[17] I. R. Fisher and J. R. Cooper, Physica C **272**, 125 (1996).

[18] M. Shepard, P. F. Hennig, G. Cao, and J. E. Crow, J. Appl. Phys. **83**, 6989 (1998).

[19] L. Ghivelder, I. Abrego Castillo, N. McN.Alford, G. J. Tomka, P. C. Riedi, J. MacManus Driscoll, A. K. M. Akther Hossain, and L. F. Cohen, J. Magn. Magn. Mater. **189**, 274 (1998).

[20] F. Damay, C. Martin, M. Hervieu, A. Maignan, B. Raveau, G. Andre, and F. Bouree, J. Magn. Magn. Mater. **184**, 71 (1998).

[21] J. P. Doumerc, J. Solid State Chem. **110**, 419 (1994).

[22] D. B. Marsh and P. E. Paris, Phys. Rev. B **54**, 16 602 (1996).

[23] J. M. D. Coey, M. Viret, K. Ounadjela, and L. Ranno, Phys. Rev. Lett. **75**, 3910 (1995).